

A Techno-Economic Framework for Cost Modeling and Revenue Opportunities in Open and Programmable AI-RAN

Gabriele Gemmi, Michele Polese, Tommaso Melodia
Institute for Intelligent Networked Systems, Northeastern University
{g.gemmi, m.polese, melodia}@northeastern.edu

Abstract—The large-scale deployment of 5G networks has not delivered the expected return on investment for mobile network operators, raising concerns about the economic viability of future 6G rollouts. At the same time, surging demand for Artificial Intelligence (AI) inference and training workloads is straining global compute capacity. AI-RAN architectures, in which Radio Access Network (RAN) platforms accelerated on Graphics Processing Unit (GPU) share idle capacity with AI workloads during off-peak periods, offer a potential path to improved capital efficiency. However, the economic case for such systems remains unsubstantiated. In this paper, we present a techno-economic analysis of AI-RAN deployments by combining publicly available benchmarks of 5G Layer-1 processing on heterogeneous platforms—from x86 servers with accelerators for channel coding to modern GPUs—with realistic traffic models and AI service demand profiles for Large Language Model (LLM) inference. We construct a joint cost and revenue model that quantifies the surplus compute capacity available in GPU-based RAN deployments and evaluates the returns from leasing it to AI tenants. Our results show that, across a range of scenarios encompassing token depreciation, varying demand dynamics, and diverse GPU serving densities, the additional capital and operational expenditures of GPU-heavy deployments are offset by AI-on-RAN revenue, yielding a return on investment of up to $8\times$. These findings strengthen the long-term economic case for accelerator-based RAN architectures and future 6G deployments.

I. INTRODUCTION

Over the past decade, mobile network operators have completed large-scale fifth generation (5G) deployments, upgrading spectrum holdings, transport networks, and radio access infrastructure. Despite these investments, the expected revenue uplift has not materialized. Most operators have experienced flat or declining returns, and no transformative application has emerged to justify the capital expenditure profile of the 5G rollout [1]. As the community begins to define sixth generation (6G) system requirements, this economic misalignment highlights a structural challenge: without a new source of value creation, the incentive to undertake a further hardware refresh remains weak.

In parallel, Artificial Intelligence (AI) has become a dominant driver of global compute demand. Training and inference workloads increasingly rely on high-performance accelerators, creating sustained pressure on datacenter capacity [2]. These workloads also exhibit significant spatial and temporal variability, suggesting potential complementarity with the utilization profile of the Radio Access Network (RAN) [3]. In virtualized

and O-RAN architectures, where Layer-1 processing increasingly relies on general-purpose accelerators such as Graphics Processing Units (GPUs), the same hardware supporting the RAN may be repurposed for different compute tasks when traffic intensity is low, with utilization gains driven by statistical multiplexing.

This concept, often referred to as *AI-and-RAN* by the AI-RAN Alliance, envisions the RAN not only as a consumer of AI algorithms but also as a provider of compute resources to external tenants. Under this model, idle accelerator capacity during off-peak periods can be allocated to AI tasks (also known as *AI-on-RAN* workloads), thereby introducing a new revenue mechanism while preserving the real-time performance constraints of the radio workload. If realized at scale, such architectures may help address the economic feasibility of future 6G deployments by improving the capital efficiency of accelerator-rich RAN platforms. However, despite research and technical developments in this space [4]–[8], there are still several questions around the economics of such systems. Among others: will the revenue generated by AI-on-RAN offset the increased Capital Expenditure (CapEx) associated with powerful general purpose accelerators? *Are systems dynamics (e.g., utilization patterns over time) amenable to generating enough revenue through sharing?*

In this paper, we answer these questions by investigating the techno-economic implications of AI-RAN systems. We combine publicly available benchmarks of 5G Layer-1 processing on heterogeneous platforms, including x86 servers with Forward Error Correction (FEC) accelerators to modern GPUs, with user-driven traffic models to quantify the amount of surplus compute capacity expected in realistic deployments. We also model demand for AI services, namely, Large Language Models (LLMs), and combine the models to construct a cost and revenue model that characterizes the value of renting RAN excess capacity to AI tenants. Our results indicate that in most scenarios modeled in this paper—including token depreciation, varying demand dynamics, and diverse serving densities for LLMs on GPUs—the additional CapEx and Operational Expenditure (OpEx) introduced by GPU-heavy deployments are offset through revenue generated by AI-on-RAN services running on the shared AI-RAN infrastructure, with a return on investment of up to 8 times. This strengthens the long-term economic case for accelerator-based RAN architectures and

future 6G rollouts. We also release the software used for the techno-economic model as open source and also packaged as a webapp that can be used to reproduce the results of this paper.¹²

The remainder of this article is organized as follows. Section II surveys related work, Section III introduces the RAN architecture landscape and compares GPU-based and FEC-accelerated platforms. Section IV sizes the server cluster for a target deployment and characterizes residual capacity available for non-RAN workloads. Section V formulates the LLM inference demand model consuming this surplus. Section VI combines deployment cost and inference revenue into a unified economic framework. Section VII presents quantitative results for a dense urban deployment in Milan, Italy. Finally, Section VIII summarizes findings and discusses future directions.

II. RELATED WORK

The economic case for virtualized and open RAN has been the subject of extensive industry analysis. Analysys Mason concluded that Open RAN can deliver TCO savings of up to 30% under favorable conditions [9], and a follow-up study reported growing operator confidence, with Open RAN projected to reach 20–30% of total RAN revenues by 2028 [10], [11]. These analyses, however, evaluate the RAN compute substrate as single-purpose infrastructure and do not consider the additional revenue that idle accelerator capacity could generate.

The AI-RAN Alliance, formed in 2024 [5], introduced a framework for repurposing that idle capacity by organizing research into three pillars—AI-for-RAN, AI-on-RAN, and AI-and-RAN—with the latter targeting the coexistence of RAN and AI workloads on shared GPU hardware. Kundu et al. [6] proposed a reference architecture with a proof-of-concept on GH200 servers, establishing feasibility without addressing economics. On the orchestration side, Shah et al. [7], [8] developed the CAORA framework, which uses reinforcement learning to dynamically partition MIG resources while maintaining near-99% RAN demand fulfillment, and Polese et al. [4] extended the O-RAN Service Management and Orchestration (SMO) to support unified management of heterogeneous workloads. These contributions address the *how* of AI-RAN coexistence but leave the *whether it pays off* question unanswered.

On the demand side, Erdil [12] developed a roofline-style cost model for LLM serving that relates token throughput to hardware constraints, while Gundlach et al. [13] empirically documented quality-adjusted inference price declines of 5–10× per year. Demirel et al. [14] corroborated these trends using API transaction data from OpenRouter and Microsoft Azure, reporting approximately 1000× price declines for models at the 2023 frontier and estimating short-run price elasticities just above unity. From a model efficiency standpoint, Xiao et al. [15] introduced the concept of *capability density* and showed that the maximum capability density of open-source LLMs doubles roughly every 3.5 months, implying that inference cost per unit of capability decreases exponentially—a trend directly relevant

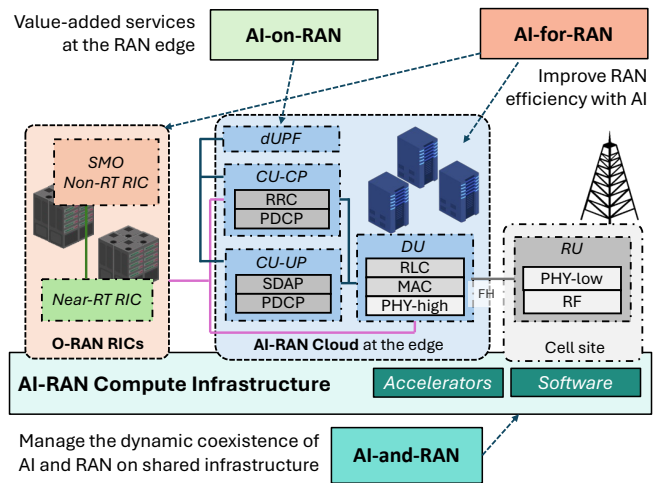


Fig. 1. AI-RAN system architecture and role of AI-for-RAN (increasing RAN efficiency and performance with AI), AI-on-RAN (value-added edge services co-deployed with the RAN and with access to RAN data and telemetry), and AI-and-RAN (orchestration and management to support the coexistence of RAN, AI-for-RAN, and AI-on-RAN).

to our ρ_{tok} parameter. The BurstGPT dataset [16], which we use to derive weekly demand profiles, provides timestamped traces of real-world LLM inference traffic.

Although edge LLM deployment has received attention from a systems efficiency perspective [17], [18], no prior work treats the RAN as a source of opportunistic inference compute or models the resulting revenue against the GPU cost premium. This paper fills that gap with a unified techno-economic framework combining platform benchmarking, demand-driven deployment sizing, and a dual-use revenue analysis.

III. RAN ARCHITECTURES AND COST MODEL

Traditional RANs rely on integrated, vendor-specific base stations in which radio, baseband processing, and control functions are tightly coupled within proprietary hardware. The 3GPP and O-RAN architectures in 5G and beyond disaggregate these functions into distinct logical components: the Radio Unit (RU) handles radio frequency operations, the Distributed Unit (DU) processes Layer-1 and Layer-2 protocol functions, and the Central Unit (CU) manages higher-layer control and user plane processing (Fig. 1). While the RU is usually based on Field Programmable Gate Arrays (FPGAs) or dedicated hardware, the DU and CU open opportunities for software-based implementations deployed on general purpose compute [19], [20].

AI-RAN extends this architecture by explicitly designing the compute substrate to support both real-time Layer-1 processing and batch or inference AI-on-RAN workloads from external AI tenants. The key enabler is the use of high-performance accelerators, such as GPUs, whose resources can be dynamically allocated to RAN functions (e.g., during peak traffic periods) and to AI tasks (e.g., during idle intervals). The economic viability of this dual-use model depends critically on the baseband capacity, cost, and power efficiency of the underlying hardware platforms, which we characterize below.

¹Repo: www.github.com/wineslab/AIRAN-revenue-model

²Webapp: www.open6g.us/#/ai-ran-economics

TABLE I
SUMMARY OF SERVER CHARACTERISTICS, BASEBAND CAPACITY, AND ECONOMIC EFFICIENCY

Platform	Accel.	Layer 1	Cost (\$)	Power (W)	L DL/UL	N_C	BW (MHz)	B (MHz)	η_C (MHz/\$)	η_O (MHz/W)	Ref.
ARS-111GL	GH200	Aerial	45000	1200	4/4	40	100	16000	0.36	13.33	[21]
ARS-111GL	GH200	Aerial	45000	1200	16/8	6	100	9600	0.21	8.00	[22]
mixed 3:1 w. avg.	GH200	Aerial	45000	1200	–	–	–	14400	0.32	12.00	
EGX74I	VRB1	FlexRAN	6000	300	16/8	6	100	9600	1.60	32.00	[23]
EGX74I	VRB1	FlexRAN	6000	300	4/4	36	10	1440	0.24	4.80	[23]
DL110	VRB1	FlexRAN	7200	300	4/4	18	20	1440	0.20	4.80	[24]
DL110	VRB1	FlexRAN	7200	300	16/8	6	100	9600	1.33	32.00	[24]
mixed 3:1 w. avg.	VRB1	FlexRAN	6600	300	–	–	–	3480	0.70	11.60	

A. Baseband Capacity Metric

To compare platforms with heterogeneous Multiple Input, Multiple Output (MIMO) layers, cell count, and bandwidth configurations under a single metric, we define the baseband capacity B [MHz] as the aggregate downlink baseband processing capacity:

$$B = L_{DL} \times N_C \times BW, \quad (1)$$

where L_{DL} is the number of downlink MIMO layers, N_C is the number of simultaneously served cells, and BW is the channel bandwidth per cell in MHz. This product captures the total spatial-frequency processing load sustained by a baseband processor (e.g., a server) and provides the basis for two economic efficiency indicators. Capital efficiency relates baseband capacity to the server acquisition cost: $\eta_C = \frac{B}{\text{Cost}}$ while power efficiency relates it to the platform power consumption: $\eta_O = \frac{B}{\text{Power}}$. Therefore, the first represent a component of CapEx, while the second contributes to OpEx.

B. Platform Comparison

Table I summarizes the baseband processing capacity and economic efficiency of representative server platforms from publicly available benchmarks and vendor specifications. The platforms are grouped by Layer-1 software stack: NVIDIA Aerial [25], which targets GPU-based architectures using the GH200 Grace Hopper Superchip, and Intel FlexRAN [26], which leverages the VRB1 FEC accelerator [27] on x86 server platforms. The literature and technical specifications for both platforms [25]–[27] identifies two representative cell configurations as benchmarks: a *macro-cell* with up to 16 MIMO layers transmitted through a mMIMO frontend, and a *micro-cell* with 4 MIMO layers transmitted through a low-order antenna panel.

The GPU-based ARS-111GL achieves 9600 MHz in the macro-cell configuration and up to 16 GHz in micro-cell mode, both at a platform cost of \$45000 and 1200 W power draw. The VRB1-based FlexRAN platforms (EGX74I at \$6000 and DL110 at \$7200, both at 300 W) reach 9600 MHz in the macro-cell configuration—matching the GPU in raw baseband throughput—at a fraction of the cost and power. As discussed

in [26], [27], for the micro-cell mode reference solution, capacity drops to 1440 MHz with correspondingly lower efficiency.

In a realistic dense urban deployment, macro and micro cells coexist. Following ITU-R deployment guidelines [28], we adopt a 1:3 macro-to-micro cell ratio for the remainder of the analysis. The deployment-weighted average baseband capacity per server is:

$$\bar{B} = \frac{B_{\text{macro}} + 3B_{\text{micro}}}{4}. \quad (2)$$

For Aerial, $\bar{B}_{\text{Aerial}} = 14400$ MHz, while for FlexRAN, $\bar{B}_{\text{FlexRAN}} = 3480$ MHz. Despite Aerial’s higher absolute capacity, FlexRAN achieves a superior CapEx efficiency: $\eta_C^{\text{FlexRAN}} \approx 0.70$ MHz/\$ versus $\eta_C^{\text{Aerial}} \approx 0.32$ MHz/\$. This is because Aerial’s sevenfold cost premium outweighs its fourfold capacity advantage in the mixed deployment, making FlexRAN the more capital-efficient baseband platform—absent the dual-use revenue considered in the following sections.

To translate these per-server metrics into deployment costs, we dimension each stack to deliver an aggregate peak throughput of 10 Gbps—assuming $SE = 9$ bit/s/Hz and 20% L1/L2 overhead—and compute the 10-year Total Cost of Ownership (TCO), reflecting a typical mobile network investment cycle.

Figure 2 reports the resulting CapEx, OpEx, and TCO broken down by cell type and platform stack. In the macro-cell configuration, FlexRAN achieves the lowest TCO thanks to its high per-server capacity at low cost and power. In the micro-cell and mixed 3:1 deployments, the gap narrows as the higher cell count reduces FlexRAN’s efficiency advantage. However, the economic case for AI-RAN rests not on baseband cost alone but on the *dual-use* capability of GPU hardware: during off-peak hours, the GPU can be repurposed for AI inference workloads—an option unavailable to dedicated FEC accelerators. The higher acquisition cost of GPU platforms must therefore be weighed against the additional revenue they can generate from surplus compute, which we quantify in the following sections.

IV. RAN DEMAND AND DEPLOYMENT MODEL

We develop a general model for sizing an AI-RAN deployment given a target geographic area and population density,

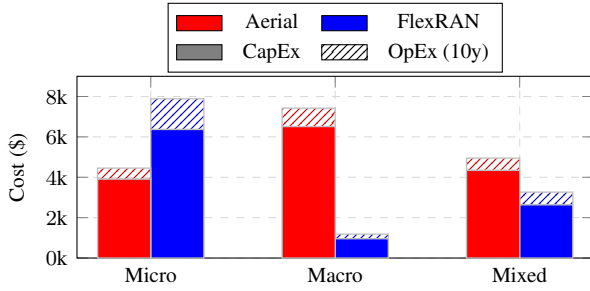


Fig. 2. TCO for 10 Gbps aggregate peak throughput over 10 years.

deriving the number of servers required, their associated capital and operational costs, and the residual compute capacity available for AI workloads. The model is anchored to the International Mobile Telecommunication (IMT)-2030 (6G) capability targets defined in International Telecommunication Union (ITU)-R Recommendation M.2160 [29], which sets a per-user experienced downlink rate of 300–500 Mbps for the immersive communication usage scenario—a $3\times$ improvement over the IMT-2020 requirement of 100 Mbps [30]. Since no outdoor dense urban area traffic capacity target has been finalized for IMT-2030 at the time of writing, we adopt a user-demand-driven approach to derive the required area capacity.

We model the per-user downlink rate $R_{\text{user}}(w, h)$ as the product of a long-term growth trend and a normalized hourly demand profile $\lambda_{\text{RAN}}(h) \in [0, 1]$, with $\max_h \lambda_{\text{RAN}}(h) = 1$ at the busy hour:

$$R_{\text{user}}(w, h) = R_{\text{user}}(0) \cdot \rho_{\text{R}}^{w/52} \cdot \lambda_{\text{RAN}}(h) \quad [\text{Mbps}], \quad (3)$$

where w is the week index (with $w = 0$ at deployment), $h \in \{0, \dots, 23\}$ is the hour of day, ρ_{R} is the annual RAN demand growth factor, and $R_{\text{user}}(0)$ is the baseline busy-hour rate from IMT-2030 (e.g., 300 Mbps). Given a deployment area with population density ρ_{pop} , the downlink demand per unit area at week w , hour h is:

$$D_{\text{area}}(w, h) = \rho_{\text{pop}} \cdot \eta_{\text{pen}} \cdot \alpha_{\text{BH}} \cdot R_{\text{user}}(w, h) \quad [\text{Mbps}/\text{km}^2], \quad (4)$$

where η_{pen} is the smartphone penetration and α_{BH} is the busy-hour concurrency factor.

To translate this demand into a server count, each platform provides an average baseband capacity \bar{B} (defined in Eq. (1)), computed as the mean across the benchmark configurations of the selected Layer-1 stack (Table I). After accounting for average spectral efficiency and L1/L2 signaling overhead η_{OH} (DeModulation Reference Signal (DMRS), Channel State Information - Reference Signal (CSI-RS), Synchronization Signal Block (SSB), Physical Random Access Channel (PRACH), guard bands), the net deliverable downlink throughput per server is:

$$C_{\text{net}} = \bar{B} \cdot \text{SE} \cdot (1 - \eta_{\text{OH}}) \quad [\text{Mbps}]. \quad (5)$$

For a target deployment area A [km^2], we denote by $G^{\text{RAN}}(w, h)$ the number of GPUs (servers) required for RAN at week w , hour h :

$$G^{\text{RAN}}(w, h) = \left\lceil \frac{A \cdot D_{\text{area}}(w, h)}{C_{\text{net}}} \right\rceil. \quad (6)$$

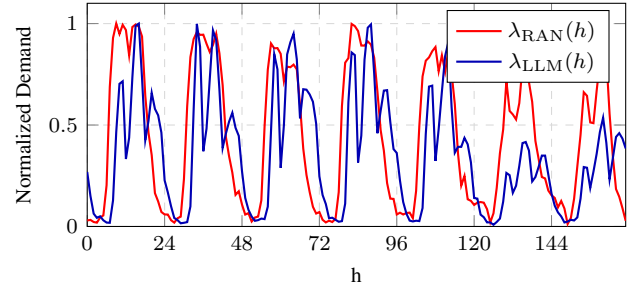


Fig. 3. Weekly usage patterns for RAN and LLM workloads showing slightly complementary demand cycles.

The physical deployment is fixed at the dimensioning week w_{dim} and busy hour h_{peak} (e.g., $w_{\text{dim}} = 0$ to size for launch, or $w_{\text{dim}} = W$ to over-provision for end-of-horizon demand). Let $G^{\text{RAN}}(w_{\text{dim}}, h_{\text{peak}})$ denote the dimensioned cluster size. The CapEx is:

$$C = G^{\text{RAN}}(w_{\text{dim}}, h_{\text{peak}}) \cdot \text{Cost}_{\text{server}} \quad [\$], \quad (7)$$

The weekly profile $\lambda_{\text{RAN}}(h)$, derived from empirical urban macro-cell measurements [31], is shown in Fig. 3. Because $G^{\text{RAN}}(w, h)$ already encodes both demand growth and hourly variation, we define the weekly OpEx as:

$$O(w) = \sum_{h=0}^{23} G^{\text{RAN}}(w, h) \cdot \frac{P_{\text{server}} \cdot \text{PUE}}{1000} \cdot c_{\text{elec}}, \quad (8)$$

where P_{server} is the server TDP in watts and the factor $1/1000$ converts to kilowatts.

Because the cluster is dimensioned to a fixed peak, servers are partially idle at all other times and their spare capacity is available for AI workloads. The number of GPUs $G_{\text{free}}(w, h)$ available for AI at week w , hour h is:

$$G_{\text{free}}(w, h) = G_{\text{total}} - G^{\text{RAN}}(w, h) \quad (9)$$

when $\rho_{\text{R}} = 1$ or $w = w_{\text{dim}}$, this reduces to $G_{\text{free}}(h) = G_{\text{total}} - G^{\text{RAN}}(w_{\text{dim}}, h)$.

V. LLM DEMAND MODEL

We model the LLM inference demand that can be served by the AI-RAN cluster during off-peak RAN hours. The workload is characterized by three parameters: the market token price p_{tok} [\$/token], the per-GPU output throughput T_{GPU} [tok/s], and the maximum sustainable request concurrency per GPU ρ_{max} [req/GPU]. All three depend on the specific LLM and hardware platform and are instantiated for a concrete model in Section VII. Following Xiao et al. [15], we introduce a *density scaling* parameter ρ_{dens} (annual capability density growth factor) that captures the growth of LLM capability density over time: the same hardware delivers more capable output as models improve. The effective per-GPU throughput at week w is then

$$T_{\text{GPU}}(w) = T_{\text{GPU}}(0) \cdot \rho_{\text{dens}}^{w/52} \quad [\text{tok}/\text{s}], \quad (10)$$

where $T_{\text{GPU}}(0)$ is the baseline throughput at deployment ($w = 0$).

To characterize temporal demand patterns and per-request workload, we use the BurstGPT dataset [32], a real-world trace of LLM inference requests containing timestamped records with input token counts. From this trace we extract two quantities: (i) a raw hourly request count $\lambda_{\text{LLM}}(h)$ that captures the weekly shape of inference demand, and (ii) the average number of tokens per request \bar{T}_{req} . Because the trace does not identify individual users, we cannot directly estimate per-user request rates from it. Instead, we derive the baseline per-user daily request rate $\bar{q}(0)$ from public ChatGPT usage statistics: with approximately 2.5–3 billion prompts processed daily across 190.6 million daily active users [33], the ratio yields $\bar{q}(0) \approx 14.4$ req/user/day.

We model the per-user daily request rate as a time-varying quantity $\bar{q}(w)$ that compounds at the annual growth factor ρ_{LLM} :

$$\bar{q}(w) = \bar{q}(0) \cdot \rho_{\text{LLM}}^{w/52} \quad [\text{req/user/day}], \quad (11)$$

where w is the week index. We rescale the BurstGPT hourly profile so that its daily per-user average matches $\bar{q}(w)$. Normalizing the raw counts gives the weekly shape $\hat{\lambda}_{\text{LLM}}(h) = \lambda_{\text{LLM}}(h) / \sum_{h=0}^{23} r(h)$, representing the fraction of daily requests that fall in hour h . The number of LLM-active users in the deployment area is $A \cdot \rho_{\text{pop}} \cdot \eta_{\text{pen}} \cdot \eta_{\text{AI}}$. The hourly request arrival rate at week w , hour h is then

$$\Lambda(w, h) = \frac{\hat{\lambda}_{\text{LLM}}(h)}{3600} \cdot \bar{q}(w) \cdot A \cdot \rho_{\text{pop}} \cdot \eta_{\text{pen}} \cdot \eta_{\text{AI}} \quad [\text{req/s}]. \quad (12)$$

The profile $\lambda_{\text{LLM}}(h)$ is shown alongside $\lambda_{\text{RAN}}(h)$ in Fig. 3. The two curves are *partially anti-correlated*: the morning RAN peak coincides with the LLM demand trough, and the evening LLM peak coincides with declining RAN load, with the primary conflict window between 14:00 and 18:00. This complementarity is favorable for dual-use server scheduling (without considering de-synchronized curves based on different markets or geographical areas).

Given that each request requires on average \bar{T}_{req} tokens to process, the mean service time per request at week w is $\bar{s}(w) = \bar{T}_{\text{req}} / T_{\text{GPU}}(w)$. Applying Little’s Law to the inference queue, the mean number of concurrently active requests at week w , hour h is $L(w, h) = \Lambda(w, h) \cdot \bar{s}(w)$, and the number of GPUs required to sustain the full demand is:

$$G_{\text{req}}^{\text{LLM}}(w, h) = \left\lceil \frac{L(w, h)}{\rho_{\text{max}}} \right\rceil = \left\lceil \frac{\Lambda(w, h) \cdot \bar{T}_{\text{req}}}{T_{\text{GPU}}(w) \cdot \rho_{\text{max}}} \right\rceil \quad (13)$$

Specific parameter values and the user scenarios evaluated in this paper are detailed in Section VII.

VI. REVENUE MODEL FOR AI-ON-RAN

The AI-RAN revenue model combines the RAN deployment cost (Section IV) with the incremental income generated by renting surplus compute to LLM inference consumers. At each week w , hour h , the number of GPUs available for AI workloads is $G_{\text{free}}(w, h)$ (Eq. (9)). The LLM allocation $G_{\text{alloc}}^{\text{LLM}}(w, h)$ is capped by the instantaneous LLM demand from Section V:

$$G_{\text{alloc}}^{\text{LLM}}(w, h) = \min(G_{\text{req}}^{\text{LLM}}(w, h), G_{\text{free}}(w, h)). \quad (14)$$

TABLE II
SCENARIO PARAMETERS – MILAN DENSE URBAN DEPLOYMENT.

Parameter	Symbol	Value	Ref.
<i>RAN demand</i>			
Population density	ρ_{pop}	7500 /km ²	[34]
Smartphone penetration	η_{pen}	80%	[35]
Busy-hour concurrency	α_{BH}	10%	[36]
Per-user downlink rate	$R_{\text{user}}(0)$	300 Mbps	[29]
Avg. spectral efficiency	SE	9 bit/s/Hz	[37]
L1/L2 overhead	η_{OH}	20%	[38]
Power Usage Effectiveness	PUE	1.5	[39]
Electricity cost	c_{elec}	0.20 \$/kWh	[40]
RAN demand growth factor	ρ_{R}	1.2	[41]
<i>LLM inference (Llama 3.1 70B 8-bit Floating Point (FP8))</i>			
Per-GPU output throughput	$T_{\text{GPU}}(0)$	37 tok/s	[42]
Max concurrency per GPU	ρ_{max}	23.5 req/GPU	[43]
Avg. tokens per request	\bar{T}_{req}	969.17	[32]
Per-user daily requests	$\bar{q}(0)$	14.4 req/day	[33]
Token price	p_{tok}	0.88 \$/Mtok	[44]
Token depreciation	ρ_{tok}	0.5	[14]
LLM adoption ratio	η_{AI}	50%	[45]
LLM demand growth factor	ρ_{LLM}	16	[14]

The resulting token throughput delivered to inference consumers at week w , hour h is:

$$T(w, h) = G_{\text{alloc}}^{\text{LLM}}(w, h) \cdot \rho_{\text{max}} \cdot T_{\text{GPU}}(w) \quad [\text{tok/s}]. \quad (15)$$

Tokens are priced at a market rate p_{tok} [\$/token]. Motivated by the empirical price trends documented by Demiret et al. [14], we model token price erosion through a depreciation factor $\rho_{\text{tok}} \in (0, 1]$, where $p_{\text{tok}}(w) = p_{\text{tok}} \cdot \rho_{\text{tok}}^{w/52}$; Over a deployment lifetime of W weeks, the total LLM revenue is thus:

$$R_{\text{LLM}}(w) = 7 \cdot p_{\text{tok}}(w) \cdot \sum_{h=0}^{23} T(w, h) \cdot 3600 \quad (16)$$

and the total LLM revenue over the deployment lifetime is

$$R_{\text{LLM}} = \sum_{w=0}^{W-1} R_{\text{LLM}}(w). \quad (17)$$

The net economic gain of the AI-RAN investment over a conventional RAN-only deployment is then the difference between R_{LLM} and the additional CapEx premium of GPU platforms over dedicated FEC-accelerator alternatives, amortized over the deployment lifetime. Scenario-specific parameter choices and the resulting revenue projections are presented in Section VII.

VII. SCENARIO-BASED EVALUATION

We instantiate the models of Sections IV–VI for a dense urban deployment in Milan, Italy. Table II summarizes the RAN and LLM parameters used across all scenarios. Throughout the evaluation, we consider two dimensioning strategies for the AI-RAN cluster:

- **Scenario 1:** the cluster is sized for launch demand, $w_{\text{dim}} = 0$, with RAN demand held constant over the 10-year lifetime ($\rho_{\text{R}} = 1$).
- **Scenario 2:** the cluster is sized for end-of-horizon demand, $w_{\text{dim}} = W$, with RAN demand growing at $\rho_{\text{R}} = 1.2$.

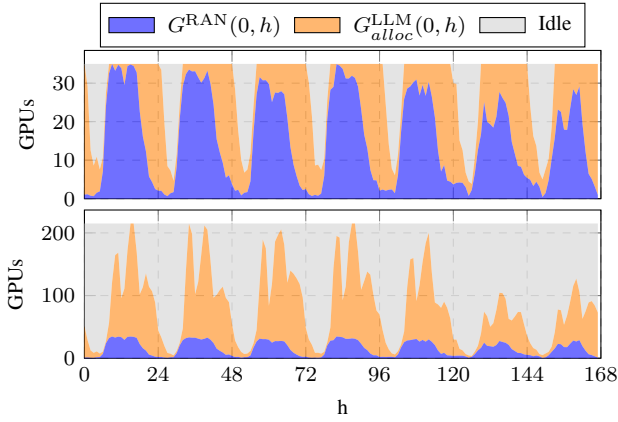


Fig. 4. Hourly GPU allocation at deployment ($w = 0$) for clusters sized for Scenario 1 (top) and Scenario 2 (bottom). The total deployed capacity G_{total} is split at each hour between RAN processing and LLM inference.

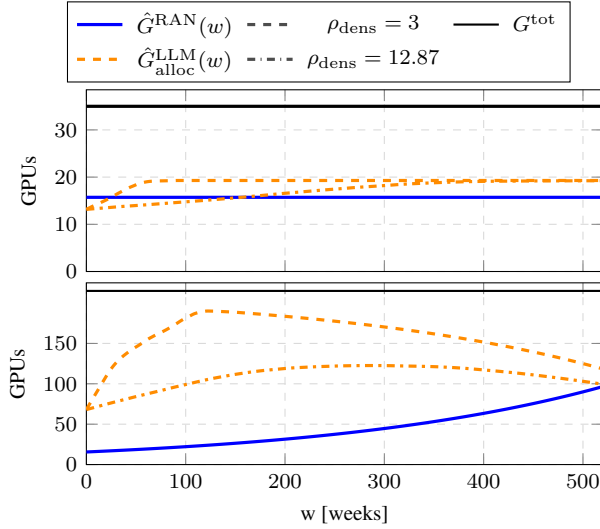


Fig. 5. Weekly-averaged GPU allocation (RAN plus LLM) over the 10-year horizon. Top: Scenario 1. Bottom: Scenario 2.

A. GPUs Allocation

Figure 4 illustrates the hourly GPU allocation at deployment ($w = 0$) under both dimensioning strategies, when considering the NVIDIA Aerial deployment. In Scenario 1 (top panel), the cluster is sized to cover the weekly busy-hour peak, so little surplus remains for the LLM tenant; inference revenue is thus limited to hours when the RAN load is low. In Scenario 2 (bottom panel), the cluster is provisioned for end-of-horizon demand. At $w = 0$, RAN traffic is well below the dimensioning point, so the workload occupies only a fraction of the deployed capacity at any hour, and the surplus $G_{\text{free}}(0, h)$ is large—particularly during off-peak hours. As w increases toward w_{dim} , RAN demand absorbs a growing share of this surplus, progressively reducing the headroom available for AI tenants.

In order to evaluate the weekly-averaged GPU allocation, we define $\hat{G}(w) = 1/168 \cdot \sum_h G(w, h)$, where 168 is the number of hours in a week. $\hat{G}(w)$ is traced for both LLM and RAN in Figure 5 across the full 10-year horizon. In Scenario 1, RAN demand is constant and consumes on average

15 GPU throughput; LLM demand grows until it saturates the excess capacity after roughly four years, then plateaus at approximately 33 GPUs. In Scenario 2, the dynamics are richer. At deployment, the RAN workload occupies about 15 GPUs; as traffic grows at 20%/year, its allocation rises to roughly 100 GPUs by the end of the horizon.

For the LLM metric, different values of ρ_{dens} are explored, as there is still no consensus of what this ratio is and will be. The first one ($\rho_{\text{dens}} = 3$) has been estimated by Gundlach et al, based on the price reduction [13], while the second one ($\rho_{\text{dens}} = 12.87$) has been estimated by [15] by fitting an exponential model on the performance of different LLMs. The ρ_{dens} parameter significantly modulates both the peak allocation and its timing. Under $\rho_{\text{dens}} = 3$, slower performance densification translates into a steeper demand curve: in Scenario 2, the LLM allocation reaches approximately 190 GPUs as early as year two and a half, before declining as the RAN workload progressively absorbs the shared capacity. With $\rho_{\text{dens}} = 12.87$, efficiency gains more effectively offset demand growth, keeping the peak near 122 GPUs around year five and producing a gentler subsequent decline. In Scenario 1, the contrast manifests in the rate of saturation rather than the ceiling: the low-densification case fills the available excess capacity in roughly two years, while the high-densification case approaches the same ceiling only gradually over the full ten-year horizon.

B. LLM Revenues

To characterize the interplay between token price deflation and performance densification, we define the ratio $k = \rho_{\text{tok}}/\rho_{\text{dens}}$, which captures the relative speed at which token prices erode with respect to the efficiency gains achieved through model densification. In practice, these two quantities are structurally coupled: the market-observed token price deflation is largely driven by the very efficiency improvements that ρ_{dens} tracks, making their ratio the natural quantity to parametrize. We evaluated the revenue metric under both ρ_{dens} values considered above ($\rho_{\text{dens}} = 3$ and $\rho_{\text{dens}} = 12.87$) and found only marginal differences in the resulting revenue trajectories; accordingly, the remainder of the analysis fixes $\rho_{\text{dens}} = 12.87$ and sweeps k directly.

Figure 6 illustrates how LLM revenue evolves over the deployment horizon across different values of k . The case $k=1$ represents the neutral point at which token price deflation is exactly offset by efficiency gains, so the effective per-token price remains constant over time. For $k>1$, deflation outpaces efficiency improvement and the effective price erodes monotonically. In Scenario 1 (top panel), all curves start at approximately \$6000/week. The $k=1$ case grows steadily as the LLM workload fills the available excess capacity, reaching a plateau of roughly \$8750/week after about 92 weeks; beyond this inflection, the curve remains flat for the rest of the horizon since neither the effective token price nor the GPU allocation change further. For $k>1$, however, revenue declines from the very first week: token price deflation erodes earnings faster than the growing GPU allocation can compensate. The decline accelerates once the capacity headroom is exhausted at the same

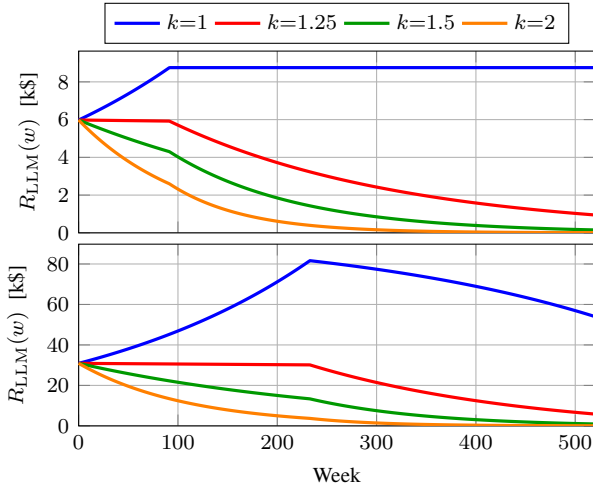


Fig. 6. Weekly LLM gross revenue over the deployment lifetime under different values of $k = \rho_{\text{tok}}/\rho_{\text{dens}}$ (token depreciation relative to efficiency improvement). Top: Scenario 1. Bottom: Scenario 2.

inflection point, since the partial offsetting effect of additional GPU hours disappears. By the end of the ten-year horizon, the $k=2$ curve is reduced to a negligible fraction of its initial value, with $k=1.5$ and $k=1.25$ following the same qualitative trend at progressively slower rates.

In Scenario 2 (bottom panel), starting from approximately \$31000/week, the $k=1$ curve grows continuously for roughly five years—peaking near \$80000/week around week 257—before declining as the expanding RAN workload progressively reclaims shared GPU hours. For $k>1$, revenue falls from the outset; beyond week 257 the loss of GPU capacity further compounds the token price erosion, steepening the decline for all curves. Crucially, the $k=2$ curve approaches zero by the end of the horizon, revealing a structural threshold: when token price deflation outpaces efficiency gains by a factor of two, LLM operation becomes economically non-viable regardless of the available infrastructure.

C. ROI Analysis

To determine whether the LLM co-tenant justifies the AI-RAN cost premium, we frame the problem as a marginal investment analysis. Let C^{Aerial} and C^{FlexRAN} denote the CapEx of each platform (Eq. (7)). The marginal investment is the additional CapEx required to deploy Aerial over the FEC-accelerated alternative:

$$I = C^{\text{Aerial}} - C^{\text{FlexRAN}}. \quad (18)$$

The cumulative net return is the gross LLM revenue minus the Aerial operational cost over the deployment horizon:

$$R(w) = R_{\text{LLM}}(w) - O(w)^{\text{Aerial}}. \quad (19)$$

Break-even is reached when cumulative R equals I ; the ratio R/I quantifies the return multiple over the full horizon.

Figure 7 shows the CapEx breakdown for Aerial and FlexRAN under both dimensioning strategies. We focus on CapEx here because the OpEx depends on the actual LLM demand: under RAN-only operation, servers are power-gated

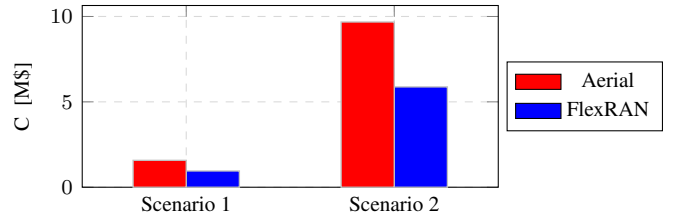


Fig. 7. CapEx for the Milan network for Aerial and FlexRAN under Scenario 1 and Scenario 2.

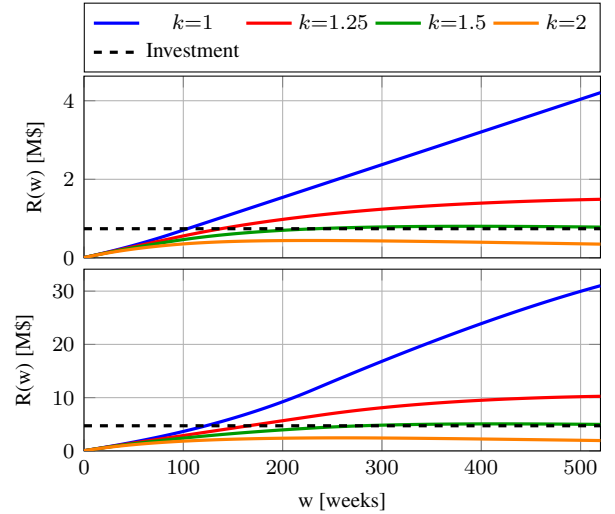


Fig. 8. Cumulative LLM revenue R (Eq. (19)) over the deployment horizon under different values of $k = \rho_{\text{tok}}/\rho_{\text{dens}}$. Top: Scenario 1. Bottom: Scenario 2. The horizontal dashed line indicates the marginal investment I (Eq. (18)).

during low-traffic periods (e.g., overnight), so the incremental energy expenditure is directly tied to the LLM workload and is therefore accounted for in the net return R (Eq. (19)). In Scenario 1, Aerial requires a CapEx of \$1.58M against \$0.95M for FlexRAN, placing the marginal investment at $I \approx \$0.62\text{M}$. In Scenario 2, the gap widens substantially: \$9.68M versus \$5.87M, yielding $I \approx \$3.80\text{M}$. This premium is a direct consequence of the GPU-based server architecture, whose per-unit acquisition cost significantly exceeds that of the FPGA-accelerated FlexRAN hardware. Transitioning from Scenario 1 to Scenario 2 increases CapEx by 514% for Aerial and 518% for FlexRAN, since the cluster must be sized for end-of-horizon demand from day one. The trade-off is that this overprovisioning creates a large pool of idle GPU hours from the outset, substantially enlarging the window for LLM revenue generation throughout the deployment lifetime.

Figure 8 plots cumulative revenue alongside the investment threshold for each scenario. The qualitative pattern mirrors the weekly revenue analysis: curves with lower k accumulate faster and recover the investment sooner, while higher k leads to slower accumulation or outright failure to break even. In Scenario 1 (top panel), the $k=1$ curve crosses the threshold at approximately week 105 (two years into deployment), followed by $k=1.25$ around week 139. The $k=1.5$ curve requires nearly the full horizon to recover the investment, crossing only

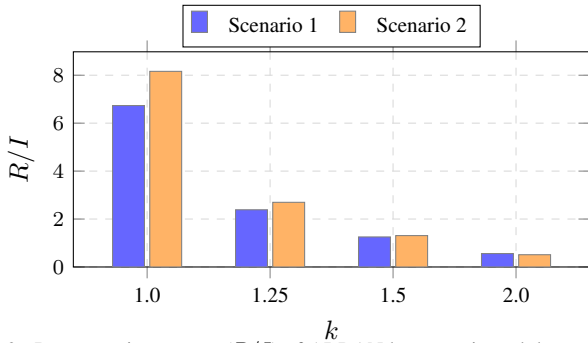


Fig. 9. Return on investment (R/I) of AI-RAN by scenario and depreciation ratio $k = \rho_{\text{tok}}/\rho_{\text{dens}}$. Investment I and return R defined in Eqs. (18) and (19).

around week 235. The $k=2$ curve never reaches break-even: the cumulative revenue at week 520 (\$0.35M) falls far short of the \$0.62M threshold, confirming that token deflation at twice the rate of efficiency improvement makes the investment irrecoverable on this timescale. In Scenario 2 (bottom panel), the investment threshold is substantially higher at \$3.80M, yet the larger volume of idle GPU capacity available from the start allows all curves except $k=2$ to cross it within the horizon. The $k=1$ curve breaks even around week 123, $k=1.25$ around week 166, and $k=1.5$ recovers the investment near week 280. As in Scenario 1, the $k=2$ case fails to break even: despite generating \$1.94M in cumulative revenue, it does not reach the \$3.80M threshold, as the compounding effect of token deflation and shrinking GPU availability forecloses recovery.

Figure 9 summarises the final return multiple R/I across all depreciation scenarios. The central finding is that Scenario 2 consistently outperforms Scenario 1 in all cases where the investment is profitable: at $k=1$, the return multiple reaches $8.2\times$ in Scenario 2 versus $6.7\times$ in Scenario 1, and at $k=1.25$ the figures are $2.7\times$ and $2.4\times$, respectively. This advantage stems directly from the deliberate over-provisioning of Scenario 2: by dimensioning the cluster for end-of-horizon demand, the operator creates an infrastructure surplus that can be leased for LLM inference from day one, generating revenue that far exceeds the additional CapEx. At $k=1.5$, both scenarios remain marginally profitable ($R/I \approx 1.31\times$ and $1.25\times$), confirming that moderate token deflation can still be offset by the efficiency gains embedded in k . At $k=2$, both scenarios yield $R/I < 1$ ($0.56\times$ and $0.51\times$), establishing a hard threshold: when token price erosion outpaces efficiency improvement by a factor of two, the LLM co-tenancy fails to recover the infrastructure premium regardless of the dimensioning strategy. Notably, the $k=2$ return is slightly lower in Scenario 2 than in Scenario 1, because the larger investment denominator more than offsets the additional revenue generated by the excess capacity.

VIII. CONCLUSION

This paper presented a techno-economic framework for evaluating AI-RAN deployments in which GPU-accelerated baseband platforms share idle capacity with LLM inference workloads. By combining publicly available hardware benchmarks, IMT-2030-anchored demand models, and empirical LLM traffic traces, we constructed a unified cost and revenue model and

instantiated it for a dense urban deployment in Milan, Italy. The analysis compared two dimensioning strategies: sizing the cluster for launch demand (Scenario 1) and for end-of-horizon demand (Scenario 2); across a range of token depreciation-to-densification ratios k .

Three principal findings emerge. For all $k \leq 1.5$, the cumulative inference revenue exceeds the marginal cost premium of the GPU-based platform, with return multiples up to $8.2\times$. Deliberate over-provisioning (Scenario 2) consistently outperforms conservative dimensioning, as the early-year surplus generates substantial revenue before RAN demand absorbs the excess capacity. The ratio $k = \rho_{\text{tok}}/\rho_{\text{dens}}$ emerges as the decisive parameter: at $k \geq 2$, the investment becomes irrecoverable regardless of dimensioning strategy, establishing a clear viability boundary for AI-RAN economics.

Several limitations of the current analysis suggest directions for future work. The revenue model prices inference tokens at prevailing cloud market rates and does not capture the additional value that edge-local inference may command: lower latency for interactive applications, reduced backhaul and transport costs for both the RAN operator and the LLM tenant, and data locality advantages for privacy-sensitive workloads. Incorporating an edge premium into the token price would likely strengthen the economic case further. The LLM demand model assumes a single workload type (LLMs); incorporating heterogeneous AI workloads such as image generation, embedding computation, or fine-tuning jobs would broaden the revenue base and potentially smooth the demand profile. Finally, the analysis also assumes a single geographic market with synchronized RAN and LLM diurnal patterns; in practice, operators serving multiple time zones or offering compute to geographically dispersed AI tenants could exploit additional temporal diversity. Despite these simplifications, the framework provides a principled and extensible basis for operators and policymakers to assess the economic viability of accelerator-based RAN architectures in the transition to 6G.

REFERENCES

- [1] GSMA Intelligence, “Global mobile trends 2023,” 2023, accessed: 2025-06. [Online]. Available: <https://www.gsma.com/>
- [2] McKinsey Global Institute, “The economic potential of generative AI: The next productivity frontier,” McKinsey & Company, Tech. Rep., Jun. 2023, accessed: 2025-06. [Online]. Available: <https://www.mckinsey.com/capabilities/mckinsey-digital/our-insights/the-economic-potential-of-generative-ai-the-next-productivity-frontier>
- [3] Y. Wang, Y. Chen *et al.*, “BurstGPT: A real-world workload dataset to optimize LLM serving systems,” in *Proceedings of the 31st ACM SIGKDD Conference on Knowledge Discovery and Data Mining (KDD '25)*. Toronto, ON, Canada: ACM, 2025. [Online]. Available: <https://doi.org/10.1145/3711896.3737413>
- [4] M. Polese, N. Mohamadi *et al.*, “Beyond connectivity: An open architecture for AI-RAN convergence in 6G,” *IEEE Communications Magazine (to appear)*, 2025. [Online]. Available: <https://arxiv.org/abs/2507.06911>
- [5] AI-RAN Alliance, “Industry leaders form AI-RAN alliance,” 2024, mWC Barcelona. [Online]. Available: <https://ai-ran.org/news/industry-leaders-in-ai-and-wireless-form-ai-ran-alliance/>
- [6] L. Kundu, X. Lin *et al.*, “AI-RAN: Transforming RAN with AI-driven computing infrastructure,” *arXiv preprint arXiv:2501.09007*, 2025. [Online]. Available: <https://arxiv.org/abs/2501.09007>

- [7] S. D. A. Shah, Z. Nezami *et al.*, “The interplay of AI-and-RAN: Dynamic resource allocation for converged 6G platform,” *arXiv preprint arXiv:2503.07420*, 2025. [Online]. Available: <https://arxiv.org/abs/2503.07420>
- [8] S. D. A. Shah, M. Hafeez *et al.*, “Proactive AI-and-RAN workload orchestration in O-RAN architectures,” *arXiv preprint arXiv:2507.09124*, 2025. [Online]. Available: <https://arxiv.org/abs/2507.09124>
- [9] Analysys Mason, “Open RAN TCO analysis,” Tech. Rep., 2022, commissioned by Wind River. [Online]. Available: https://www.analysismason.com/contentassets/b3260036a0d449718117eeaf5ac83472/analysys_mason_open_ran_tco_feb2022_rma16_rma18.pdf
- [10] —, “Open RAN progress drives confidence,” Tech. Rep., 2024, commissioned by Wind River. [Online]. Available: https://www.analysismason.com/contentassets/a99b7d01b9e64a2cafc375459c99de99/analysys_mason_open_ran_confidence_apr2024_rma18.pdf
- [11] S. Pongratz, “Open RAN and vRAN revenue trends,” 2024, dell’Oro Group. [Online]. Available: <https://www.fierce-network.com/modernization/open-ran-and-vran-tanks-2023>
- [12] E. Erdil, “Inference economics of language models,” *arXiv preprint arXiv:2506.04645*, 2025. [Online]. Available: <https://arxiv.org/abs/2506.04645>
- [13] H. Gundlach, J. Lynch *et al.*, “The price of progress: Algorithmic efficiency and the falling cost of AI inference,” *arXiv preprint arXiv:2511.23455*, 2025. [Online]. Available: <https://arxiv.org/abs/2511.23455>
- [14] M. Demirer, A. Fradkin *et al.*, “The emerging market for intelligence: Pricing, supply, and demand for LLMs,” 2025, working paper. [Online]. Available: https://andreyfradkin.com/assets/LLM_Demand_12_12_2025.pdf
- [15] C. Xiao, J. Cai *et al.*, “Densifying law of LLMs,” *Nature Machine Intelligence*, vol. 7, pp. 1823–1833, 2025.
- [16] Y. Wang, Y. Chen *et al.*, “BurstGPT: A real-world workload dataset to optimize LLM serving systems,” *arXiv preprint arXiv:2401.17644*, 2024. [Online]. Available: <https://arxiv.org/abs/2401.17644>
- [17] G. Cai, R. Tian *et al.*, “Efficient inference for edge large language models: A survey,” *Tsinghua Science and Technology*, vol. 31, no. 3, pp. 1365–1380, 2026.
- [18] D. Ding, A. Mallick *et al.*, “Hybrid LLM: Cost-efficient and quality-aware query routing,” in *Proc. ICLR*, 2024. [Online]. Available: <https://openreview.net/forum?id=02f3mUtqnM>
- [19] A. Kelkar and C. Dick, “NVIDIA Aerial GPU hosted AI-on-5G,” in *Proc. IEEE 4th 5G World Forum (5GWF)*, 2021, pp. 64–69.
- [20] A. Garcia-Saavedra and X. Costa-Perez, “O-RAN: Disrupting the virtualized RAN ecosystem,” *IEEE Communications Standards Magazine*, vol. 5, no. 4, pp. 96–103, 2021.
- [21] NVIDIA, “Enabling the world’s first GPU-accelerated 5G Open RAN for NTT DOCOMO with NVIDIA Aerial,” 2023, accessed: 2025-12. [Online]. Available: <https://developer.nvidia.com/blog/enabling-the-worlds-first-gpu-accelerated-5g-open-ran-for-ntt-docomo-with-nvidia-aerial/>
- [22] —, “Aerial CUDA-accelerated RAN release 25-2,” 2025, accessed: 2025-12. [Online]. Available: <https://docs.nvidia.com/aerial/cuda-accelerated-ran/25-2/aerial-cuda-accelerated-ran.pdf>
- [23] Quanta Cloud Technology, “QCT VRB100 vRAN server specifications,” 2024, vendor specifications; Accessed: 2025-12. [Online]. Available: <https://www.qct.io/>
- [24] Intel and Hewlett Packard Enterprise, “Verified reference configuration for virtualized RAN on the HPE ProLiant DL110,” 2022, accessed: 2025-12. [Online]. Available: <https://builders.intel.com/docs/networkbuilders/intel-hpe-verified-reference-configuration-for-virtualized-radio-access-networks-on-the-hpe-proliant-dl110-1653673153.pdf>
- [25] A. Kelkar and C. Dick, “Nvidia aerial gpu hosted ai-on-5g,” in *2021 IEEE 4th 5G World Forum (5GWF)*. IEEE, 2021, pp. 64–69.
- [26] C. Wang, H. Nie *et al.*, “Understanding 5G Performance on Heterogeneous Computing Architectures,” *IEEE Communications Magazine*, vol. 63, no. 3, pp. 107–113, March 2025.
- [27] Intel Corporation, “Intel accelerates 5G leadership with new products,” 2023, accessed: 2025-12. [Online]. Available: <https://www.intc.com/news-events/press-releases/detail/1606/intel-accelerates-5g-leadership-with-new-products>
- [28] ITU-R, “Report ITU-R M.2412-0: Guidelines for evaluation of radio interface technologies for IMT-2020,” International Telecommunication Union, Tech. Rep., Oct. 2017, dense Urban-eMBB; Accessed: 2025-06. [Online]. Available: https://www.itu.int/dms_pub/itu-r/opb/rep/R-REP-M.2412-2017-PDF-E.pdf
- [29] —, “Recommendation ITU-R M.2160-0: Framework and overall objectives of the future development of IMT for 2030 and beyond,” International Telecommunication Union, Tech. Rep., Nov. 2023, accessed: 2025-06. [Online]. Available: https://www.itu.int/dms_pubrec/itu-r/rec/m/R-REC-M.2160-0-202311-1!!PDF-E.pdf
- [30] —, “Report ITU-R M.2410-0: Minimum requirements related to technical performance for IMT-2020 radio interface(s),” International Telecommunication Union, Tech. Rep., Nov. 2017, accessed: 2025-06. [Online]. Available: <https://www.itu.int/pub/R-REP-M.2410>
- [31] G. Barlacchi, M. De Nadai *et al.*, “A multi-source dataset of urban life in the city of Milan and the Province of Trentino,” *Scientific Data*, vol. 2, p. 150055, 2015. [Online]. Available: <https://doi.org/10.1038/sdata.2015.55>
- [32] Y. Wang, Y. Chen *et al.*, “BurstGPT: A real-world workload dataset to optimize LLM serving systems,” *arXiv preprint arXiv:2401.17644*, 2024. [Online]. Available: <https://arxiv.org/abs/2401.17644>
- [33] R. A. Lee, “Claude vs. ChatGPT statistics 2026: Head-to-head numbers behind the AI battle,” 2025, 2.5–3B prompts/day, 190.6M DAU; Accessed: 2025-10. [Online]. Available: <https://sqmagazine.co.uk/claude-vs-chatgpt-statistics/>
- [34] ISTAT, “Resident population and population density – municipality of Milan,” 2024, population density $\approx 7\,500/\text{km}^2$; Accessed: 2025-06. [Online]. Available: <https://www.istat.it/en/>
- [35] GSMA Intelligence, “The state of mobile internet connectivity 2024,” 2024, accessed: 2025-06. [Online]. Available: <https://data.gsmainelligence.com/research/research/2024/the-state-of-mobile-internet-connectivity-2024>
- [36] J. Lorincz and Z. Klarin, “A comprehensive analysis of the impact of an increase in user devices on the long-term energy efficiency of 5G networks,” *Smart Cities*, vol. 7, no. 6, pp. 3616–3657, 2024. [Online]. Available: <https://www.mdpi.com/2624-6511/7/6/140>
- [37] ITU-R WP 5D, “Preliminary draft new report ITU-R M.[IMT-2030.TECH PERF REQ]: Minimum requirements related to technical performance for IMT-2030 radio interface(s),” International Telecommunication Union, Tech. Rep., 2024, working document; Accessed: 2025-06.
- [38] 3GPP, “TS 38.214: NR; physical layer procedures for data (release 18),” 3rd Generation Partnership Project, Tech. Rep., 2024, accessed: 2025-06. [Online]. Available: <https://www.3gpp.org/dynareport/38214.htm>
- [39] Uptime Institute, “2024 global data center survey: Report,” 2024, accessed: 2025-06. [Online]. Available: <https://datacenter.uptimeinstitute.com/rs/711-RIA-145/images/2024.GlobalDataCenterSurvey.Report.pdf>
- [40] Eurostat, “Electricity price statistics,” 2024, household and industrial prices; 0.3291 EUR/kWh; Accessed: 2025-06. [Online]. Available: https://ec.europa.eu/eurostat/statistics-explained/index.php?title=Electricity_price_statistics
- [41] Ericsson, “Ericsson mobility report,” Tech. Rep., November 2025, accessed: February 23, 2026. [Online]. Available: <https://www.ericsson.com/4aca6f/assets/local/reports-papers/mobility-report/documents/2025/ericsson-mobility-report-november-2025.pdf>
- [42] Artificial Analysis, “LLM performance leaderboard: Model and API provider benchmarks,” 2024, accessed: 2025-06. [Online]. Available: <https://artificialanalysis.ai/leaderboards/models>
- [43] J. Pichlmeier, P. Ross, and A. Luckow, “Performance characterization of expert router for scalable LLM inference,” in *arXiv preprint arXiv:2404.15153*, 2024. [Online]. Available: <https://arxiv.org/abs/2404.15153>
- [44] Together AI, “Together AI – inference pricing,” 2024, llama 3.3 70B: \$0.88/Mtok; Accessed: 2025-06. [Online]. Available: <https://www.together.ai/pricing>
- [45] B. Savoldi, G. Attanasio *et al.*, “Generative ai practices, literacy, and divides: An empirical analysis in the italian context,” 2025. [Online]. Available: <https://arxiv.org/abs/2512.03671>